Four-port integrated polarizing beam splitter

Zhan Su,[1,*] Erman Timurdogan,[1] Ehsan Shah Hosseini,[1] Jie Sun,[1] Gerald Leake,[2] Douglas D. Coolbaugh,[2] and Michael R. Watts[1]

[1]*Research Laboratory of Electronics, Massachusetts Institute of Technology, Cambridge, Masschusetts 02139, USA*

[2]*College of Nanoscale Science and Engineering, University at Albany, Albany, New York 12203, USA*

**Corresponding author: zhansu@mit.edu*

Received November 18, 2013; revised December 22, 2013; accepted January 5, 2014; posted January 7, 2014 (Doc. ID 201495); published February 11, 2014

In this Letter, we report on the first integrated four-port polarizing beam splitter. The device operates on the principle of mode evolution and was implemented in a silicon-on-insulator silicon photonics platform and fabricated on a 300 mm CMOS line using 193 nm optical immersion lithography. The adiabatic transition forming of the structure enabled over a 150 nm bandwidth from $\lambda \sim 1350$ to $\lambda \sim 1500$ nm, achieving a cross-talk level below −10 dB over the entire band. © 2014 Optical Society of America

OCIS codes: (130.3120) Integrated optics devices; (130.2790) Guided waves; (230.5440) Polarization-selective devices.

http://dx.doi.org/10.1364/OL.39.000965

Recently, the development of CMOS-compatible silicon photonic platforms has been spurred by the exponentially increasing demand for bandwidth within the Internet and within the data centers that empower it. Integrated silicon photonics [1] offer single-mode operation, unprecedented bandwidth density, and compactness that can leverage Moores law scaling [2] for off-chip communications and even within the chip (e.g., intra-chip) communications. While communications are driving the current interest in silicon photonics, the resulting silicon photonic platforms can be applied to numerous problems, ranging from sensing and phased arrays to microwave photonics and quantum optics, often achieving degrees of performance that cannot be achieved with their free-space optic counterparts [3,4]. Yet the general applicability of these platforms is determined by how extensive their component libraries are and how easily free-space optical trains can be implemented. From active components such as modulators [5], detectors [6], and even lasers [7] to passive components such as 3 dB couplers [8] and waveguide crossings [9], component libraries within silicon photonics platforms are becoming increasingly general, yet they remain incomplete. One critical component missing from these libraries is the polarizing beam splitter (PBS).

On account of the polarization dependence caused by the use of high-index contrast materials such as silicon and silicon nitride (Si_3N_4) within silicon photonics, polarization components were developed [10,11] and realized [12] early on to enable polarization-independent operation. Yet while components such as polarization splitters [13–16], polarization rotators [17], and integrated polarization splitter-rotators [18,19] have been demonstrated on silicon platforms, an on-chip equivalent of a free-space PBS has not previously been demonstrated. All "so-called" PBS demonstrated so far, with 10 dB extinction bandwidths of 50, 60, 70, and 100 nm [13–16], are in themselves polarization splitters, with only one input and two outputs and not true four-port beam splitters. Though devices based on directional couplers [15,16] can, in principle, both separate and combine polarization states, adiabatic structures do so with larger bandwidths and fabrication tolerances [10–12].

A true PBS requires a two-input two-output configuration. Though applications for on-chip polarization-insensitive photonic circuits and polarization multiplexing schemes [20] generally only require the use of one-input two-output polarization splitters, for more intricate systems such as polarization-entangled state generation, manipulation, and detection in quantum optics [21] or heterodyne interferometers [22], a fully functional two-input two-output PBS is required.

In this Letter, we designed and demonstrated a broadband mode-evolution-based PBS implemented on a silicon photonics platform and fabricated on a 300 mm silicon-on-insulator (SOI) wafer with a 220 nm device layer, using 193 nm optical immersion lithography. The silicon PBS, the first reported fully functional integrated PBS (two input and two output ports), operates over a 150 nm bandwidth with less than −10 dB cross talk. Importantly, this device provides a substantial addition to the component library with immediate application to compact on-chip interferometers and quantum information processing.

The operation of a traditional PBS reflects the transverse electric (TE) component while transmitting the transverse magnetic (TM) field component as depicted in Fig. 1(a), where the orientation of the field is defined relative to the plane of incidence (i.e., plane of the page). To realize the same functionality on-chip, we propose the adiabatic structure depicted in Fig. 1(b). Note that in the standard convention for waveguide optics, the TE polarization is in the chip plane while TM polarization is orthogonal to that plane. Stated otherwise, in a modal sense, the waveguide TM super-modes remain in their respective guides largely unaffected by the transition while the TE super-modes cross waveguides.

The structure depicted in Fig. 1(b) evolves slowly along its length. Therefore we can apply coupled local mode theory to its operation as in [11] and repeated here for convenience. In the weak-coupling limit, the coupling coefficient $\kappa_{mn}(z)$ between mode m and mode n can be expressed as

$$\kappa_{mn}(z) = \frac{\omega}{4\delta\beta}\int_A \mathbf{e}_{\mathbf{m}}^{*}(x,y,z)\cdot\mathbf{e}_{\mathbf{n}}(x,y,z)\frac{d}{dz}\varepsilon(z)\mathrm{d}A, \quad (1)$$

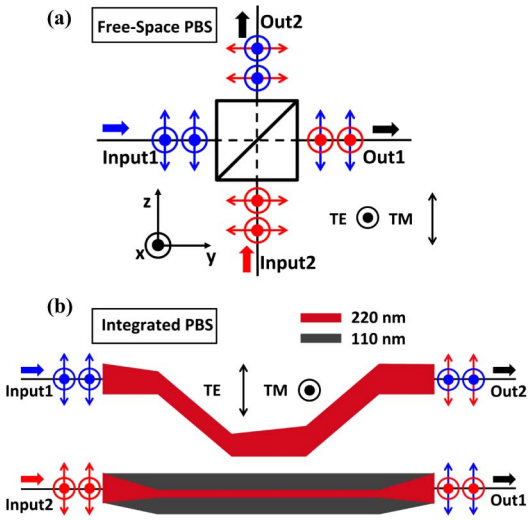

Fig. 1. (a) For comparison, the operation of a traditional free-space PBS cube is shown alongside a proposed integrated PBS (b). Note: the TE/TM polarization convention is inverted on-chip compared to the free-space case.

where $\mathbf{e_k}(x, y, z)$ stands for normalized vector electric field of mode k, $\delta\beta(z)$ is the difference in the propagation constants as a function of length z, ω is the angular frequency of the input light, $\varepsilon(z)$ is the electric permittivity as a function of length, and A is the perturbed area. Then the power transferred to mode m (P_m) from mode n can be written as

$$P_m(z) \propto 2\left|\frac{\bar{\kappa}}{\overline{\delta\beta}}\right|^2[1-\cos(\overline{\delta\beta}z)], \tag{2}$$

where $\bar{\kappa}$ is the average coupling coefficient, and $\overline{\delta\beta}$ is the average difference in the propagation constants, expressed as $\bar{\kappa} = (1/z)\int_0^z \kappa(z')\mathrm{d}z'$ and $\overline{\delta\beta} = (1/z)\int_0^z \delta\beta(z')\mathrm{d}z'$. In general, for an adiabatic transition, the ratio between $\bar{\kappa}$ and $\overline{\delta\beta}$ needs to be much smaller than 1 to ensure negligible coupling to unwanted modes. The difference in the propagation constants, $\overline{\delta\beta}$, is determined by the waveguide shape and index contrast, whereas the strength of the coupling, $\bar{\kappa}$, is determined by the shape and pace of the transition. For a given $\overline{\delta\beta}$, the ratio can be reduced by introducing a slowly varying permittivity function $\varepsilon(z)$, which minimizes $d\varepsilon(z)/dz$, and therefore longer structures are more effective at mode evolution than are their shorter counterparts. Given that the desired structure consists of two input and output ports, if each port guides a single TE and a single TM polarization, there must be four super-modes (i.e., modes of the combined structure) present at the input and the output or two for each polarization.

In order to ensure the TE super-modes cross waveguides without affecting the TM super-modes, the input waveguide is designed to contain the fundamental TE super-mode (TE_{11}) in the lower waveguide, while at the output the fundamental TE super-mode propagates in the upper waveguide, all the while leaving the TM super-modes largely unaffected. Ideally, the TE and TM super-modes would be staggered in their effective indices ($\bar{n}_{\mathrm{TE}_{11}} > \bar{n}_{\mathrm{TM}_{11}} > \bar{n}_{\mathrm{TE}_{21}} > \bar{n}_{\mathrm{TM}_{21}}$), so as to minimize coupling during the waveguide transition since similar polarized modes have much higher coupling coefficients than orthogonally polarized modes. However, due to fabrication constraints, thin silicon waveguides are preferred. These thin waveguides guide the TE polarization more effectively, precluding the desired alternating effective indices. With such thin waveguides, it becomes nearly impossible to achieve such a staggered condition. By easing the condition with a longer device, instead of staggering the effective indices of the modes, well-separated TE and TM effective indices ($\bar{n}_{\mathrm{TE}_{11}} > \bar{n}_{\mathrm{TE}_{21}} > \bar{n}_{\mathrm{TM}_{11}} > \bar{n}_{\mathrm{TM}_{21}}$) achieve the same goal. Apart from that, to satisfy the switching of TE super-modes without affecting TM super-modes, the full-thickness silicon waveguide cannot be used solely for the design, in which case both TE and TM super-modes will behave in the same manner under the adiabatic limit. Rather, structures that have different birefringence relations need to be implemented. Starting from Gauss's electric law, which provides the jump condition

$$\hat{n}\cdot(\bar{D}_1 - \bar{D}_2) = 0 \tag{3}$$

at the boundaries, causing the electric field of the TM modes of a rectangular waveguide to be discontinuous along the y direction (i.e., normal to the wafer surface) and the electric field of the TE modes to be discontinuous along the x direction (i.e., parallel to the wafer surface). For our current process, the device layer is 220 nm, and the normally used waveguide width is larger than 220 nm. Thus the TE mode will have a field discontinuity along short edges while TM mode will have it for long edges.

For a silicon rectangular waveguide with SiO_2 cladding, two factors—core material size and boundary conditions—determine the effective indices of the modes. With the same size of core material, the different boundary conditions lead to different TE and TM modes effective indices. Using a square waveguide as the starting point, perturbation theory [23] indicates that

$$\Delta\bar{n} = \frac{\bar{n}}{4}\iint \mathbf{e}_\mathbf{m}^*\cdot\mathbf{e}_\mathbf{m}\cdot\Delta\varepsilon\mathrm{d}x\mathrm{d}y, \tag{4}$$

where $\Delta\bar{n}$ is the effective index change of mode due to dielectric perturbation $\Delta\varepsilon$, $\mathbf{e_m}$ stands for normalized vector electric field of mode m, and $\bar{n}$ is the unperturbed effective index. Assuming uniform field distribution (amplitude E) inside the core region, combining boundary conditions together and taking account of the sharp index contrast [24], the effective index changes for TM and TE modes under perturbation can be expressed as

$$\Delta\bar{n}_{\mathrm{TE}} = \frac{\bar{n}}{4}(\varepsilon_c - \varepsilon_{\mathrm{cl}})E^2\left[\left(\frac{\varepsilon_c}{\varepsilon_{\mathrm{cl}}}\right)H\cdot\Delta W + W\cdot\Delta H\right], \tag{5}$$

$$\Delta\bar{n}_{\mathrm{TM}} = \frac{\bar{n}}{4}(\varepsilon_c - \varepsilon_{\mathrm{cl}})E^2\left[\left(\frac{\varepsilon_c}{\varepsilon_{\mathrm{cl}}}\right)W\cdot\Delta H + H\cdot\Delta W\right], \tag{6}$$

where ε_c and $\varepsilon_{\mathrm{cl}}$ are the core and cladding dielectric constants, and ΔW and ΔH are the width and height change of the rectangular waveguide [shown in Fig. 2(a)], which

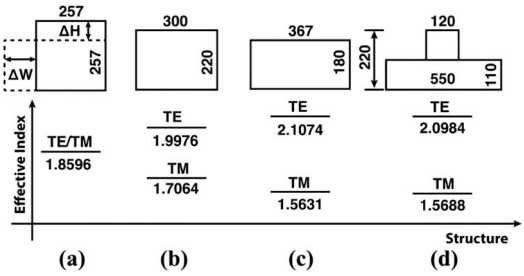

Fig. 2. Different waveguide shapes and their corresponding effective indices for TM and TE modes solved at a wavelength of 1440 nm.

are constrained by the core size. When the height of the waveguide gets decreased, $\Delta W > 0$ and $\Delta H < 0$ will affect TE and TM modes in different ways, leading to splitting of the effective indices of those modes. Figures 2(a) to (c) show three rectangular waveguides with the same core size and different widths and heights, an increase for TE mode and a decrease for TM mode on effective index are clearly indicated. With suitable deformations, different amounts of splitting can be achieved. In this manner, the effective index condition ($\bar{n}_{\mathrm{TE}_{11}} > \bar{n}_{\mathrm{TE}_{21}} > \bar{n}_{\mathrm{TM}_{11}} > \bar{n}_{\mathrm{TM}_{21}}$) can be satisfied independent of the wavelength. To achieve this ordering of effective indices, two waveguide thicknesses, 220 and 180 nm, are desired. However, due to fabrication-process limitations, only 220 and 110 nm silicon thicknesses are available. Yet, by utilizing a T-shaped waveguide, the effects of over-etching to a 110 nm layer thickness on the effective indices of those modes are compensated by adjusting the fin size and total width of the structure [shown in Fig. 2(d)] to produce a waveguide with an effective thickness of 180 nm.

The resultant PBS structure is depicted in Fig. 3(a). Two well-separated 400 nm width full-thickness input waveguides are first converted to a narrower waveguide and a ridge waveguide. The large separation ensures a smooth transition of individual modes of the waveguides without mutual coupling, which would otherwise reduce the operating bandwidth. This sets the initial condition for the effective indices to $\bar{n}_{\mathrm{TE}_{11}} > \bar{n}_{\mathrm{TE}_{21}} > \bar{n}_{\mathrm{TM}_{11}} > \bar{n}_{\mathrm{TM}_{21}}$ with the fundamental TE mode propagating in the lower waveguide and fundamental TM mode propagating in the upper waveguide [shown in the first set of mode profiles in Fig. 3(c) and start of Fig. 3(d)]. The two waveguides are then brought close to each other, and the modes of individual waveguides become super-modes of the two-waveguide system while the effective index ordering of the modes is still maintained. The full-thickness waveguide is then tapered up to 400 nm to evolve the fundamental TE super-mode to propagate in the upper waveguide while the TM super-modes remain in the same waveguides [shown in the third set of mode profiles in Fig. 3(c)]. It is important to note that the effective index ordering is maintained with relatively large effective index differences among super-modes preserved all along the propagation path. The two waveguides are then separated again adiabatically, resulting in a fundamental TE mode evolving to the upper waveguide and the secondary TE mode to the lower waveguide, while TM modes remain in their respective waveguides. In the last stage, two well-separated waveguides are then converted to

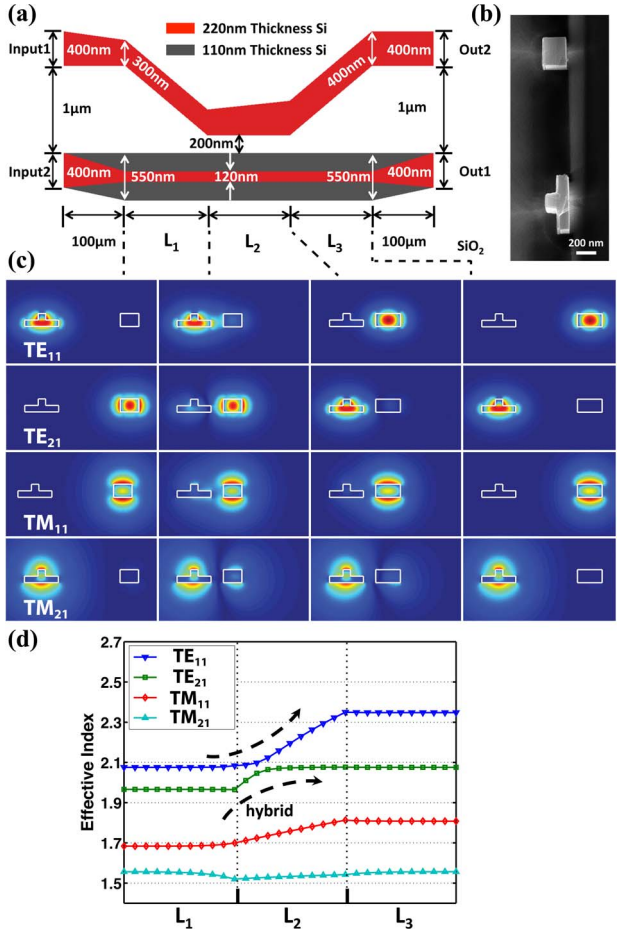

Fig. 3. (a) Schematic of the full PBS. $L_1 = L_3 = 500$ μm. $L_2 = 200$ μm. (b) Cross-sectional scanning electron microscope (SEM) image of the device within L_1 region. (c) Eigen-modes profiles for corresponding cross sections (dotted lines) of the device in order of effective indices. (d) Eigen-modes effective indices evolutions from the beginning of the L_1 part to the end of L_3 part for wavelength of 1440 nm.

a normal 400 nm width full-thickness waveguide to connect to other on-chip devices. Though adiabatic devices are generally larger in footprint than nonadiabatic ones, the larger bandwidths and fabrication tolerances make them more suitable candidates for wafer-scale fabrications.

The proposed structure was fabricated on a 300 mm SOI wafer with a 220 nm device layer and a 2 μm thick buried oxide layer using 193 nm optical immersion lithography. The device was then covered with a 3.3 μm thick top oxide layer. The cross-sectional SEM figure of the fabricated device within L_1 region is shown in Fig. 3(b). The ridge waveguide has a 110 nm ridge thickness, a 120 nm width on top, and a 550 nm width on the bottom.

The fabricated device was coupled by using an off-chip lensed single-mode-fiber (SMF), and cross- and through-transmission spectra were measured through identical-lensed SMFs. At both ends of the chip, inversely tapered waveguide couplers were used to match the waveguide mode to the fiber mode, maximizing the coupling between the fiber and the chip. An external polarization controller was used to manipulate the input polarization states, and a nearby integrated micro-ring resonator was

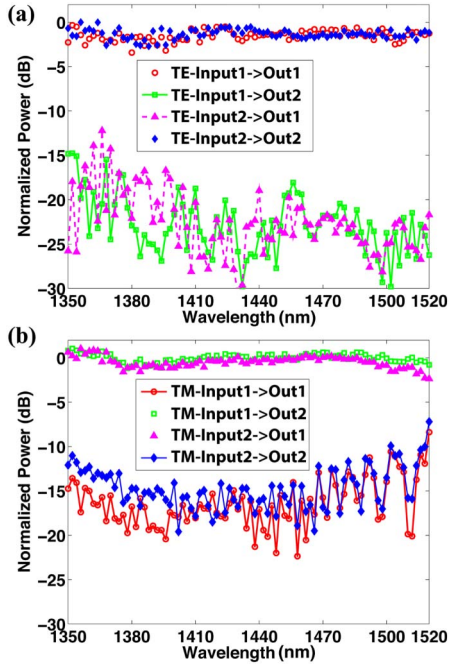

Fig. 4. Transmission spectra of the designed PBS for (a) TE-input polarization and (b) TM-input polarization from different input ports to different output ports.

used to identify polarization states for a given wavelength range. Additionally, the power for each polarization was normalized to a nearby straight waveguide with identical inversely tapered waveguide couplers. The TE modes from both input ports were excited separately, and both output ports were measured to identify cross talk. The transmission spectra from $\lambda = 1350$ to $\lambda = 1520$ nm are presented in Fig. 4(a). The TE modes, excited from either input, achieve over 170 nm bandwidth operation, with less than −10 dB cross talk and loss of 3.4 dB at maximum. Similarly, the TM mode transmission spectra are shown in Fig. 4(b), indicating over 150 nm bandwidth from $\lambda = 1350$ to $\lambda = 1500$ nm, less than −10 dB cross talk and loss of 2.6 dB at maximum. The bandwidth for the TE modes is limited by high-order-mode interaction and insufficient transition length (L_2) for $\lambda < 1350$ nm, while the TM modes are limited by the substrate leakage of TM modes for $\lambda > 1500$ nm. Thus, by performing the design steps shown in Fig. 2 with different starting sizes of the waveguide, devices that are working in other communication bands (e.g., 1310, 1550 nm) can be readily fabricated.

In conclusion, a four-port (two input and two output ports) integrated PBS is demonstrated for the first time with a record bandwidth of over 150 nm and less than −10 dB cross talk for TE and TM modes on a 300 mm CMOS-compatible SOI platform. The device provides a substantial addition to the silicon photonics component library with immediate application to compact on-chip interferometers and quantum information processing.

This work was supported in part by the Defense Advanced Research Projects Agency (DARPA) Microsystems Technology Offices (MTO) EPHI program, grant no. HR0011-12-2-0007.

References

1. M. Asghari and A. V. Krishnamoorthy, Nat. Photonics **5**, 268 (2011).
2. S. Borkar and A. A. Chien, Commun. ACM **54**, 67 (2011).
3. J. Sun, E. Timurdogan, A. Yaacobi, E. S. Hosseini, and M. R. Watts, Nature **493**, 195 (2013).
4. J. C. Matthews, A. Politi, A. Stefanov, and J. L. O'Brien, Nat. Photonics **3**, 346 (2009).
5. M. R. Watts, D. C. Trotter, R. W. Young, and A. L. Lentine, in *Proceedings of Fifth IEEE International Conference on Group IV Photonics* (IEEE, 2008), Vol. **46**, pp. 46.
6. C. T. DeRose, D. C. Trotter, W. A. Zortman, A. L. Starbuck, M. Fisher, M. R. Watts, and P. S. Davids, Opt. Express **19**, 24897 (2011).
7. Purnawirman, J. Sun, T. N. Adam, G. Leake, D. Coolbaugh, J. D. B. Bradley, E. S. Hosseini, and M. R. Watts, Opt. Lett. **38**, 1760 (2013).
8. Y. Zhang, S. Yang, A. E.-J. Lim, G.-Q. Lo, C. Galland, T. Baehr-Jones, and M. Hochberg, Opt. Express **21**, 1310 (2013).
9. W. Bogaerts, P. Dumon, D. V. Thourhout, and R. Baets, Opt. Lett. **32**, 2801 (2007).
10. M. R. Watts and H. A. Haus, Opt. Lett. **30**, 138 (2005).
11. M. R. Watts, H. A. Haus, and E. P. Ippen, Opt. Lett. **30**, 967 (2005).
12. T. Barwicz, M. R. Watts, M. A. Popović, P. T. Rakich, L. Socci, F. X. Kärtner, E. P. Ippen, and H. I. Smith, Nat. Photonics **1**, 57 (2007).
13. J. Wang and D. Dai, in *Optical Fiber Communication Conference/National Fiber Optic Engineers Conference*, 2013, paper OTh4I.1.
14. J. Wang, D. Liang, Y. Tang, D. Dai, and J. E. Bowers, Opt. Lett. **38**, 4 (2013).
15. B.-K. Yang, S.-Y. Shin, and D. Zhang, Photon. Technol. Lett. **21**, 432 (2009).
16. H. Fukuda, K. Yamada, T. Tsuchizawa, T. Watanabe, H. Shinojima, and S. Itabashi, Opt. Express **14**, 12401 (2006).
17. L. Chen, C. R. Doerr, and Y.-K. Chen, Opt. Lett. **36**, 469 (2011).
18. Y. Ding, H. Ou, and C. Peucheret, Opt. Lett. **38**, 1227 (2013).
19. W. Sacher, T. Barwicz, and J. K. Poon, in *Conference on Lasers and Electro-Optics*, 2013, paper CTu3F.3.
20. P. Dong, C. Xie, L. Chen, L. L. Buhl, and Y.-K. Chen, Opt. Express **20**, B624 (2012).
21. P. Kok, K. Nemoto, T. C. Ralph, J. P. Dowling, and G. J. Milburn, Rev. Mod. Phys. **79**, 135 (2007).
22. S. Slussarenko, V. D'Ambrosio, B. Piccirillo, L. Marrucci, and E. Santamato, Opt. Express **18**, 27205 (2010).
23. D. H. Staelin, A. W. Morgenthaler, and J. A. Kong, *Electromagnetic Waves* (Prentice-Hall, 1994).
24. S. Johnson, M. Ibanescu, M. Skorobogatiy, O. Weisberg, J. Joannopoulos, and Y. Fink, Phys. Rev. E **65**, 066611 (2002).